RESEARCH ARTICLE

# Importance of Electron Mediator Transparency: Photocatalytic Hydrogen Production from Polyoxometalate using Dye-double-layered Photocatalysts

Nobutaka Yoshimura,[a] Osamu Tomita,[b] Ryu Abe,[b] Masaki Yoshida,[c] and Atsushi Kobayashi*[a]

[a] Mr. N. Yoshimura and Dr. A. Kobayashi*
Department of Chemistry, Faculty of Science,
Hokkaido University
North-10 West-8, Kita-ku, Sapporo 060-0810, Japan
*E-mail: akoba@sci.hokudai.ac.jp (A.K.).
[b] Dr. O. Tomita and Prof. Dr. R. Abe
Department of Energy and Hydrocarbon Chemistry,
Graduate School of Engineering, Kyoto University,
Nishikyo-ku, Kyoto 615-8510, Japan
[c] Dr. M. Yoshida
Department of Applied Chemistry for Environment,
School of Biological and Environmental Sciences, Kwansei Gakuin University,
2-1 Gakuen, Sanda, Hyogo 669-1337, Japan

Supporting information for this article is given via a link at the end of the document.

**Abstract:** One-directional electron transfer is crucial for two-step photoexcitation (Z-scheme) water-splitting photocatalysis. We investigated the hydrogen evolution activity of PS-double-layered photocatalysts (**X-DSP**, X-**RuCP$^6$**-Zr-**RuP$^6$**@Pt/$K_xH_{4-x}Nb_6O_{17}$; X = $Zr^{4+}$, $H^+$) in the presence of highly charged polyoxometalates—$K_6[SiV^{IV}W_{11}O_{40}]\cdot nH_2O$ (**V$^{IV}$-POM**) and $K_6[SiW_{11}O_{39}Mn^{II}(H_2O)]\cdot nH_2O$ (**Mn$^{II}$-POM**)—as redox-reversible electron donors, to induce effective photocatalyst–donor electrostatic attraction. Surface-phosphonate-comprising **H$^+$-DSP** completely one-electron oxidized **V$^{IV}$-POM** with 0.39% apparent quantum yield in the initial hour (*i*AQY) in both HCl and phosphate buffer aqueous solutions. Conversely, the **Zr$^{4+}$-DSP** *i*AQY decreased to 0.05% in HCl aq. Considering that the 0.39% *i*AQY was retained when replacing **V$^{IV}$-POM** with **Mn$^{II}$-POM** in HCl aq, we supposed that energy transfer deactivation from photoexcited PS* to surface-immobilized **V$^{IV}$-POM** is the plausible origin of the lower *i*AQY, owing to the stronger visible-light absorptivity of **V$^{IV}$-POM**. This suggests that accumulation of visible-light-transparent electron mediator on the photocatalyst surface is an effective approach for one-directional electron transfer in Z-scheme water-splitting photocatalysis.

## Introduction

Photocatalytic water splitting has attracted considerable attention as a promising reaction to resolve the global warming and energy crises.[1-5] The use of Z-scheme photocatalysts, composed of hydrogen ($H_2$) and oxygen ($O_2$) evolution photocatalysts with an appropriate redox-reversible electron mediator, is a promising approach to ensure enough driving force for both electron transfer and catalytic reactions.[6-9] For example, Domen et al. recently reported on a Z-scheme photocatalyst composed of $ZrO_2$/TaON and $BiVO_4$ as the $H_2$ and $O_2$ evolving photocatalysts, respectively, in the presence of $[Fe(CN)_6]^{3-/4-}$ as the electron mediator. This Z-scheme system exhibited 0.6% solar-to-hydrogen (STH) energy conversion efficiency and 12.3% apparent quantum efficiency (AQY) at 420 nm.[10] However, most Z-scheme systems developed to date still suffer from the thermodynamically favorable back electron transfer processes at the photocatalyst–mediator interface. Dye-sensitized photocatalysts (DSPs) consisting of a molecular photosensitizer (PS) and semiconductor catalyst have been extensively studied to utilize visible light in the solar spectrum, accounting for approximately half of the solar light energy for $H_2$ production.[11-15] From the viewpoint of electron transfer in Z-scheme water-splitting photocatalysis, the surface modification of DSPs is an interesting and efficient method to control the electron transfer at the photocatalyst–mediator interface.[16-20] In fact, several state-of-the-art DSPs have been reported to produce $H_2$ effectively in the presence of a redox-reversible electron mediator (e.g., $I^-$ and $[Co(bpy)_3]^{2+}$) as the electron source for $H_2$ production.[21-33] Maeda et al. recently reported that the $H_2$ evolution activity of a DSP composed of a Pt-intercalated $HCa_2Nb_3O_{10}$ nanosheet and Ru(II) dye was significantly improved by surface modification with both amorphous $Al_2O_3$ and poly(styrenesulfonate) polymer, to achieve a remarkably high apparent quantum yield (AQY = 4.1% at 420 nm).[34] The origin of the high AQY was attributed to the suppression of back electron transfers from both the Pt co-catalyst and Ru(II) photosensitizer (PS) to the oxidized electron mediator, $I_3^-$, by covering the photocatalyst surface with poly(styrenesulfonate) polymer. We also reported that the surface-modified Ru(II)-PS-double-layered photocatalyst Zr-**RuCP$^6$**-Zr-**RuP$^6$**@Pt/$K_xH_{4-x}Nb_6O_{17}$ (Scheme 1; **Zr$^{4+}$-DSP**, **RuCP$^6$** = $[Ru(mpbpy)_3]^{10-}$, where **RuP$^6$** = $[Ru(pbpy)_3]^{10-}$, $H_4$mpbpy = 2,2′-bipyridine-4,4′-bis(methane-phosphonic acid), and $H_4$pbpy = 2,2′-bipyridine-4,4′-bis(phosphonic acid))[35] was highly active for $H_2$ production in the presence of redox-reversible electron donors (RREDs), such as iodide ($I^-$) anions and $[Co(bpy)_3]^{2+}$ (bpy = 2,2′-bipyridine) complex cations. Further, the surface modification drastically improved the activity owing to the electrostatic attraction of the RREDs induced by the photocatalyst surface. However, the number of active DSPs in the presence of RREDs

remains limited. Thus, new strategies for DSPs to not only suppress the back reaction but also accelerate the forward reaction at the photocatalyst–mediator interface are strongly required.

In this work, to design an efficient way to accelerate the forward electron transfer from the RRED to the photocatalyst, we selected two polyoxometalates, namely $K_6[SiV^{IV}W_{11}O_{40}]\cdot nH_2O$ and $K_6[SiW_{11}O_{39}Mn^{II}(H_2O)]\cdot nH_2O$ (**$V^{IV}$-POM** and **$Mn^{II}$-POM**, respectively), as the RREDs for photocatalytic $H_2$ production by the Ru(II)-PS-double-layered DSP, X-**RuCP$^6$**-Zr-**RuP$^6$**@Pt/$K_xH_{4-x}Nb_6O_{17}$, which is composed of Pt-cocatalyst-intercalated layered-niobate and doubly-layered Ru(II) photosensitizers (Scheme 1; **X-DSP**, X = $H^+$ and $Zr^{4+}$)[35]. These POMs were used as the electron mediator in the Z-scheme water-splitting photocatalyst because of their suitable and comparable redox potentials and superior stabilities in aqueous solution.[36-43] The important feature for this work is that these POMs are hexavalent anionic molecules, suggesting a stronger electrostatic interaction with the photocatalyst surface than that observed with commonly used electron donors. In addition, these two POMs exhibit different light absorption behaviors that significantly affect the energy transfer process with the Ru(II) PS of **X-DSP** (Figure S1). Herein, we report the photocatalytic $H_2$ evolution reaction with **X-DSP** in the presence of **$V^{IV}$-POM** and **$Mn^{II}$-POM**. **$H^+$-DSP** successfully produced $H_2$ photocatalytically until it completely oxidized a very dilute 1 mM **$V^{IV}$-POM** aqueous solution. Interestingly, the AQY in 1 mM **$V^{IV}$-POM** was comparable to those observed in higher concentrations of the other less-charged electron donors (0.5 M KI and 16 mM $[Co(bpy)_3]^{2+}$ aq).[35] In contrast, **$Zr^{4+}$-DSP** exhibited almost the same activity as **$H^+$-DSP** under phosphate buffer conditions; however, its activity remarkably decreased in HCl aq. This drop in activity in the absence of phosphate buffer was attributed to the energy transfer quenching of the photo-excited Ru(II)-PS by the electrostatically immobilized **$V^{IV}$-POM** on the **$Zr^{4+}$-DSP** surface $Zr^{4+}$ cations. This hypothesis was supported by the result that **$Zr^{4+}$-DSP** maintained its high activity in the presence of visible-light-transparent **$Mn^{II}$-POM** electron donor solution.

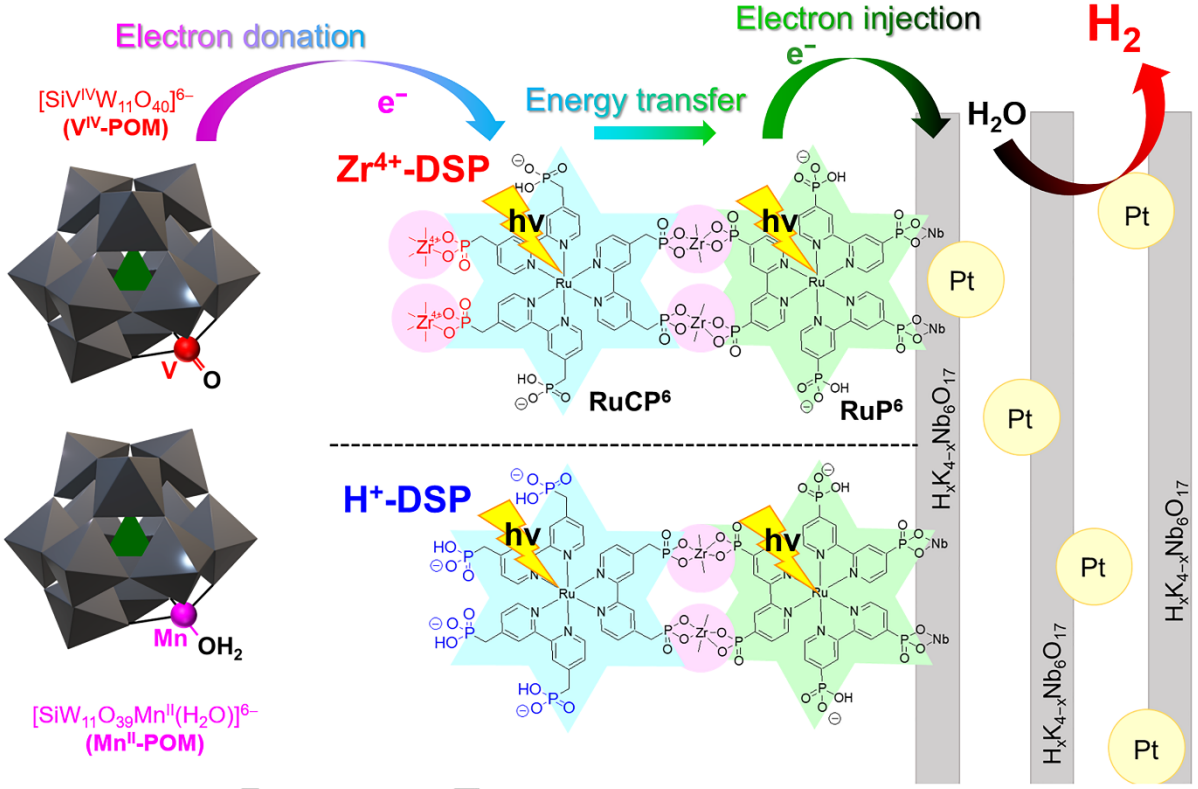


**Scheme 1.** Schematic illustration of photocatalytic $H_2$ production by **X-DSP**s with redox-reversible M-POM (M = $V^{IV}$, $Mn^{II}$) electron donors.

## Results and Discussion

### Photocatalytic $H_2$ evolution reaction

Figures 1(a) and 1(b) show the results of the photocatalytic $H_2$ evolution reactions in 1 mM **$V^{IV}$-POM** aqueous solution using **$H^+$-DSP** and **$Zr^{4+}$-DSP** as the photocatalyst, respectively. The estimated turnover numbers and frequencies per one photosensitizing dye (PS TON and PS TOF, respectively) together with the apparent quantum yield (AQY) are listed in Table 1. The total amount of Ru(II) dye in each solution was constant (100 mM) and no $H_2$ evolution was observed in the absence of Ru(II) dye, light, or electron donor (Table S2). Although **$H^+$-DSP** exhibited near-identical activities in the HCl and phosphate buffer aqueous solutions, in the early stage (<1 h), the activity in HCl aq was slightly higher than that in the phosphate buffer (Figure 1(a)). The produced amount of $H_2$ after 3 h reaction (~2.5 μmol) corresponded with the expected value when all **$V^{IV}$-POM** donors were one-electron oxidized to form **$V^{V}$-POM**. On the other hand, **$Zr^{4+}$-DSP** produced only 1.2 μmol of $H_2$ after 6 h irradiation in the HCl aq., whereas it generated almost the same amount of $H_2$ (~2.5 μmol) as did **$H^+$-DSP** after 3 h reaction in the phosphate buffer solution. The photocatalytic $H_2$ evolution was restarted by the addition of another 5 μmol of **$V^{IV}$-POM** (Figure S3), and the supernatant solutions after these reactions afforded UV-vis absorption spectra similar to that of the one-electron oxidized form, **$V^{V}$-POM** (Figure S4). These results indicate that **$V^{IV}$-POM** acted as the electron donor of the photocatalytic $H_2$ evolution reactions

with **H⁺-DSP** and **Zr⁴⁺-DSP**. Notably, the absorption bands of the Ru dyes were hardly observed in the supernatant spectra (Figure S4), suggesting the negligible desorption of these dyes. Negligible XRF spectral change of **Zr⁴⁺-DSP** by immersing to the phosphate buffer solution (Figure S5) suggests that the surface-immobilized $Zr^{4+}$ cations were hardly removed during the photocatalytic $H_2$ evolution reaction. The observed photocatalytic activity in the second cycle experiment of **H⁺-DSP** was approximately 30% less (PS TOF = 5.16) than that of the first cycle (7.51) (Figure S3). This was attributed to the presence of some back reactions related to the one-electron oxidized **$V^{V}$-POM**. Considering that the $^3$MLCT emission of $[Ru(bpy)_3]^{2+}$ was strongly quenched by **$V^{V}$-POM** (Figure S6), the back electron transfer process from the photo-excited $Ru^{2+*}$ PS to **$V^{V}$-POM** was suggested as a plausible back reaction. The AQY values for the initial hour of reaction (*i*AQY) of **H⁺-DSP** and **Zr⁴⁺-DSP** in phosphate buffer were estimated to be almost identical (0.39%), indicating no dependence on the surface structure of the photocatalytic nanoparticles in the phosphonate buffer. These *i*AQY values were also comparable to that in 0.5 M KI aq (pH = 2, *i*AQY = 0.60%) and 20 mM $[Co(bpy)_3]^{2+}$ aq (pH = 2, *i*AQY = 0.56%),[35] even though the reaction conditions—a slightly basic pH and lower donor concentration ([**$V^{IV}$-POM**] = 1 mM, pH = 3, *i*AQY = 0.39%)—were less favorable for the $H_2$ evolution reaction. Thus, we supposed that redox-reversible POM species are potential materials as electron mediators for dye-sensitized Z-scheme water splitting systems. In contrast, the *i*AQY value of **Zr⁴⁺-DSP** in HCl aq was approximately 87% lower (*i*AQY = 0.050%) than that in the phosphate buffer. To reveal the origin of this lower activity, **H⁺-DSP** and **Zr⁴⁺-DSP** were analyzed by XRF analysis, in the solid state, after photocatalytic $H_2$ evolution reaction (Figure 2).

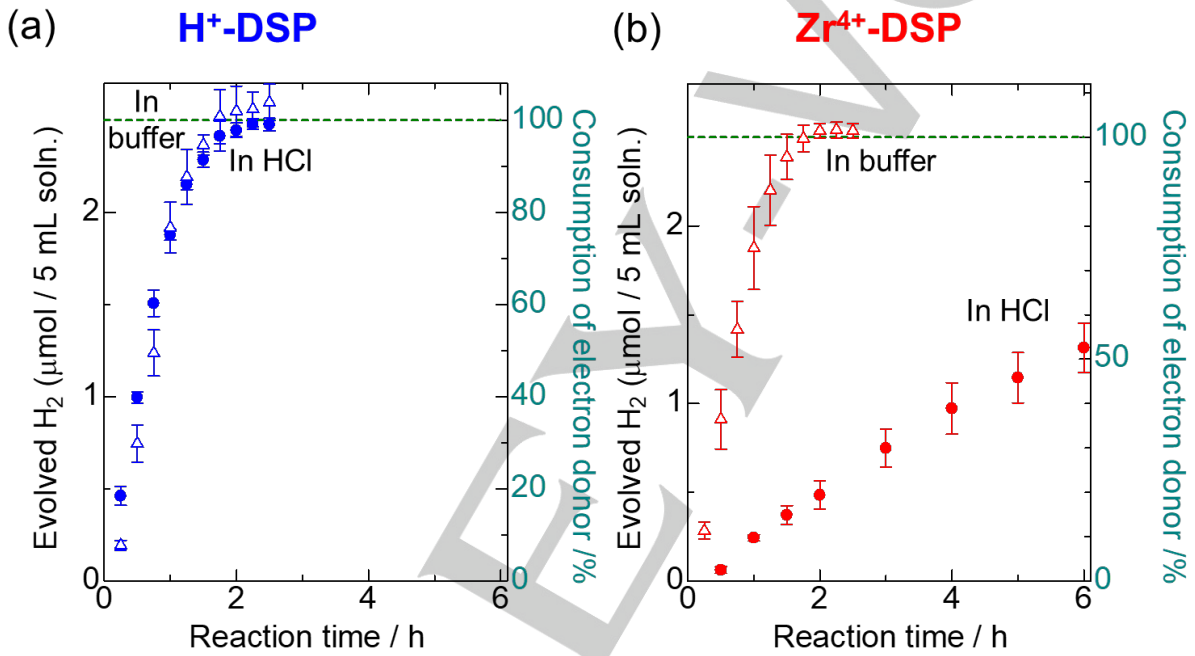


**Figure 1.** Photocatalytic $H_2$ evolution reactions driven by (a) **H⁺-DSP** and (b) **Zr⁴⁺-DSP** in the presence 1 mM **$V^{IV}$-POM** as the RRED (closed circles) in HCl aqueous solution and (open triangles) in 40 mM phosphate buffer aqueous solution. Ru(II) dye concentration of all the reactions were adjusted to 100 μM. Initial pH of all the solutions was adjusted to 3.0 by adding HCl or phosphate buffer aqueous solution (λ = 460 ± 15 nm; 70 mW).

**Table 1**. Results of photocatalytic $H_2$ evolution experiments with POM electron donor in acidic aqueous solution.

| Photocatalyst[a] | Solution | Initial pH | Electron donor | $H_2$ (μmol) (0–2 h) | PS TON[a] (0–2 h) | PS initial TOF[a] (0–1 h) | *i*AQY[a] (%) (0–1 h) |
|---|---|---|---|---|---|---|---|
| **H⁺-DSP** | Phosphate buffer | 3 | **$V^{IV}$-POM**, 1 mM | 2.55±0.18 | 10.2 | 7.67 | 0.39 |
| **H⁺-DSP** | HCl aq | 3 | **$V^{IV}$POM**, 1 mM | 2.44±0.04 | 9.78 | 7.51 | 0.39 |
| **Zr⁴⁺-DSP** | Phosphate buffer | 3 | **$V^{IV}$-POM**, 1 mM | 2.54±0.06 | 10.1 | 7.50 | 0.39 |
| **Zr⁴⁺-DSP** | HCl aq | 3 | **$V^{IV}$-POM**, 1 mM | 0.485±0.079 | 1.94 | 0.976 | 0.050 |
| **Zr⁴⁺-DSP** | HCl aq | 3 | **$Mn^{II}$-POM**, 1 mM | 2.41±0.26 | 9.62 | 7.86 | 0.40 |
| **Zr⁴⁺-DSP**[ref35] | HCl aq | 2 | KI, 0.5 M | 5.35±0.93 | 21.4 | 11.9 | 0.60 |
| **H⁺-DSP**[ref35] | HCl aq | 2 | $[Co(bpy)_3]SO_4$, 20 mM | 5.33±0.08 | 21.3 | 11.1 | 0.56 |

[a] Measurement conditions: [Ru-PS] = 100 μM in total, electron donor = 1 mM, volume = 5 mL aqueous solution, $\lambda_{ex}$ = 460 ± 15 nm, 70 mW in total. The reaction solution was purged by Ar bubbling for 1 h before light irradiation. Numeral values were an average of more than three repeated experiments. Definitions: PS = photosensitizer, PS TON = turnover number of PS, PS initial TOF = turnover frequency of PS during the initial hour of irradiation (from 0 to 1 h), *i*AQY = apparent quantum efficiency during the initial hour, **$V^{IV}$-POM** = $K_6[SiV^{IV}W_{11}O_{40}]$, **$Mn^{II}$-POM** = $K_6[SiW_{11}O_{39}Mn^{II}(H_2O)]\cdot nH_2O$.

The samples were collected by ultracentrifugation after the reaction and then completely washed twice with HCl aq (pH = 3). The XRF spectra of **$H^+$-DSP** before and after photocatalytic $H_2$ evolution reaction were almost identical (Figure 2(a)). In contrast, for **$Zr^{4+}$-DSP**, the W Lα radiation derived from **V-POM** was clearly detected after the reaction in HCl aq (Figure 2(b)) but was hardly observed in the phosphate buffer solution reaction. These results suggest that the **V-POM** species were immobilized on the surface $Zr^{4+}$ ions of **$Zr^{4+}$-DSP** during photocatalytic $H_2$ evolution in HCl aq. In the phosphate buffer solution, however, immobilization of the **V-POM** species was suppressed because of the coordination of the phosphate anions to the surface $Zr^{4+}$ cations. In fact, the zeta potential of **$Zr^{4+}$-DSP** in the HCl aq. significantly shifted negatively with the addition of **$V^{IV}$-POM** (Table S4; +31 mV → −34 mV). On the other hand, in the phosphate buffer solution, the zeta potential was largely negative even without **$V^{IV}$-POM** addition (−37 mV → −33 mV). These zeta potential changes also indicated the immobilization of **V-POM** on the **$Zr^{4+}$-DSP** surface in HCl aq. Further, the CT absorption band of **$V^{IV}$-POM** was detected in the UV-vis diffuse reflectance spectrum of **V-POM**-immobilized **$Zr^{4+}$-DSP** that was prepared by simply immersing **$Zr^{4+}$-DSP** to **$V^{IV}$-POM** aq. in the dark condition (Figure S7), implying that the oxidation state of the surface-immobilized **V-POM** species is the one-electron donatable $V^{IV}$ state.

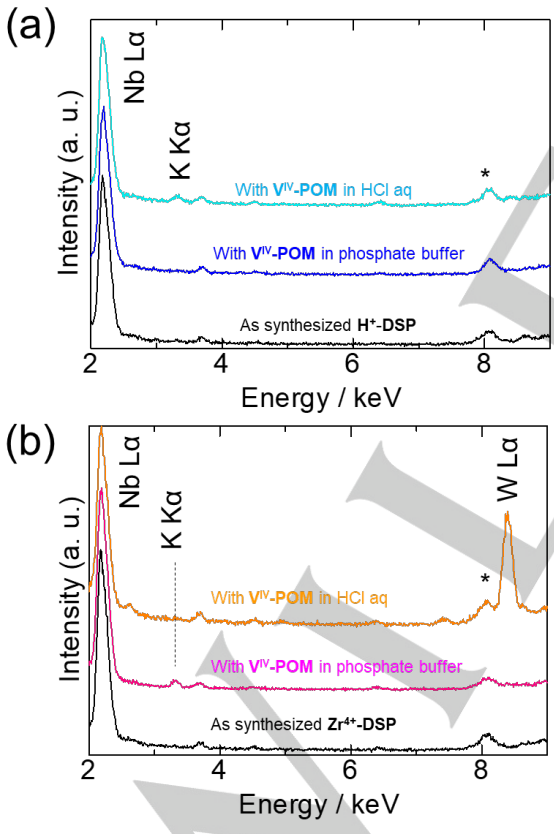


**Figure 2.** XRF spectra of (a) **$H^+$-DSP** and (b) **$Zr^{4+}$-DSP** obtained by centrifugation of the reaction solutions after photocatalytic hydrogen evolution reaction at 298 K under vacuum. All spectra were normalized with the intensity of the Nb Lα peak. The marked peak (*) is due to the background of the Cu sample holder.

As discussed above, the XRF spectra and zeta potential measurements revealed that the **V-POM** species were immobilized on the **$Zr^{4+}$-DSP** surface during the photocatalytic $H_2$ evolution reaction in HCl aq, resulting in the lower activity. As the reason why **$Zr^{4+}$-DSP** exhibited lower activity in the HCl aq condition, the energy transfer quenching of Ru dyes by **$V^{IV}$-POM** was presumed because the absorption band of **$V^{IV}$-POM** was effectively overlapped with the $^3$MLCT emission band of Ru(II) dyes (Scheme 2 and Figure S1). In fact, the $^3$MLCT emission of the simple cation $[Ru(bpy)_3]^{2+}$ was effectively quenched by **$V^{IV}$-POM**, while that of the negatively charged **RuCP$^6$**, which comprises six phosphonate groups, was hardly quenched (Figure S5). These contrasting results suggest that the electrostatic attraction between the $[Ru(bpy)_3]^{2+}$ cation and **$V^{IV}$-POM** anion effectively induce energy transfer quenching. The direct observation of the emission quenching of Ru(II) dyes in **$H^+$-DSP** and **$Zr^{4+}$-DSP** by **$V^{IV}$-POM** was difficult because of the strong light scattering of the $Pt/K_xH_{4-x}Nb_6O_{17}$ particles. However, we supposed that the surface-immobilized **V-POM** species on **$Zr^{4+}$-DSP** should induce energy transfer quenching, resulting in a lower photocatalytic activity than those of the other reaction systems in which the **V-POM** species were hardly immobilized on the DSP surface.

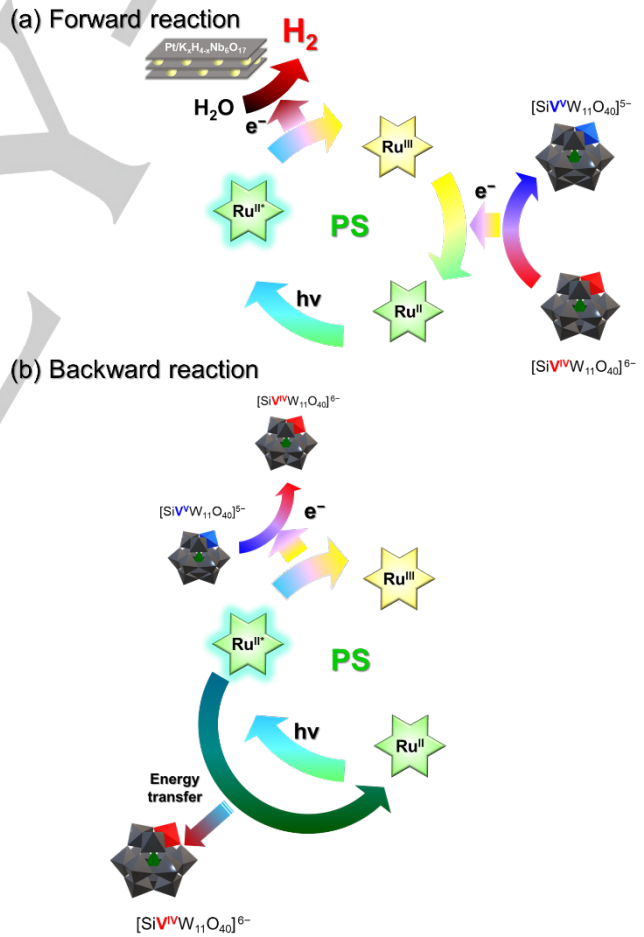


**Scheme 2.** Plausible mechanism of the (a) forward and (b) backward electron/energy transfer processes in the photocatalytic $H_2$ evolution reaction in the presence of **$V^{IV}$-POM**.

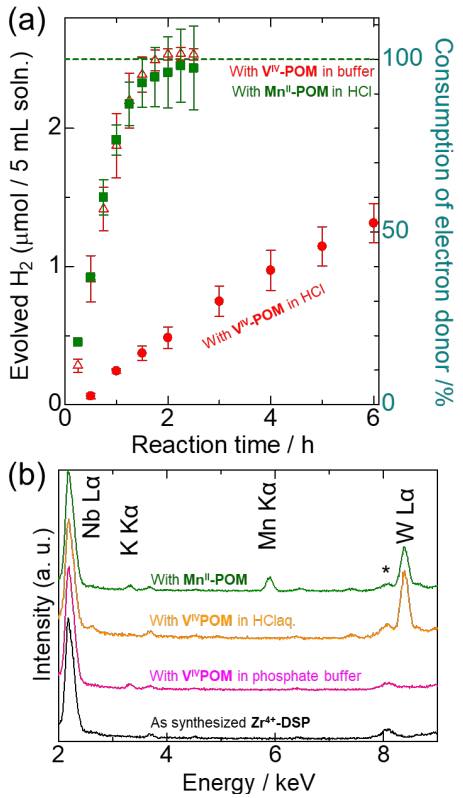


**Figure 3.** (a) Comparison of the photocatalytic $H_2$ evolution reaction driven by **$Zr^{4+}$-DSP** in the presence of 1 mM **$Mn^{II}$-POM** as the RRED in HCl aqueous solution (initial pH = 3.0) under blue light irradiation (λ = 460 ± 15 nm; 70 mW) with that of **$Zr^{4+}$-DSP** in HCl or phosphonate buffer aq. with 1 mM **$V^{IV}$-POM** RRED. (b) XRF spectra of **$Zr^{4+}$-DSP** obtained by centrifugation of the reaction solutions after photocatalytic hydrogen evolution reaction at 298 K under vacuum. All spectra were normalized with the intensity of the Nb Lα peak. The marked peak (*) is due to the background of the Cu sample holder.

To overcome the energy transfer quenching by the **$V^{IV}$-POM** electron donor, we next conducted a photocatalytic $H_2$ evolution experiment in the presence of **$Mn^{II}$-POM**, which has almost the same redox potential (+0.73 V) as **$V^{IV}$-POM**, however, without the absorptivity in the $^3$MLCT region of Ru(II) dyes (Figure S1).[36] Figure 3(a) compares these results with those of **$V^{IV}$-POM**. Interestingly, in the HCl aq. of **$Mn^{II}$-POM**, **$Zr^{4+}$-DSP** exhibited almost the same activity as that in the **$V^{IV}$-POM** solution with phosphate buffer. In the XRF spectrum of the sample obtained after the reaction (Figure 3(b)), Mn Kα radiation at 5.9 keV, which was attributed to the **Mn-POM** species, was clearly observed in addition to W Lα radiation, indicating the immobilization of **Mn-POM** to the **$Zr^{4+}$-DSP** surface, as was the case with **V-POM**. These two results indicate that **Mn-POM** species were immobilized on the **$Zr^{4+}$-DSP** surface during the photocatalytic reaction, which, however, did not decrease the photocatalytic activity. This is because the energy transfer quenching by **$Mn^{II}$-POM** is negligible. Although the electron transfer quenching of photoexcited Ru(II)* dyes by the surface-immobilized **$Mn^{II}$-** and **$V^{IV}$-POM** could be possible because of the redox reversible behavior of $W^{VI}/W^{V}$ centers in the acidic condition, this quenching pathway should not be dominant factor because of the comparable $W^{VI}/W^{V}$ potential for **$Mn^{II}$-** and **$V^{IV}$-POM**.[36] We expected that the photocatalytic activity of **$Zr^{4+}$-DSP** would be enhanced by the immobilization of **$Mn^{II}$-POM** because of the effective electron donation to the one-electron-oxidized Ru dye. In fact, the activity of **$Zr^{4+}$-DSP** in **$Mn^{II}$-POM** aq. was more than twice higher than that in the visible-light transparent electron donor KI aq. with the same 1 mM donor concentration (Figure S8). However, the estimated PS TON and AQY values were almost comparable to those of **$Zr^{4+}$-DSP** in the phosphate buffer solution, thereby preventing the surface immobilization of POM species as discussed above (Table 1). This was attributed to the low immobilization amount of the sterically bulky **$Mn^{II}$-POM**, as suggested by the XRF spectrum, that is, only 6% of the $Zr^{4+}$ sites were occupied by the **Mn-POM** species.

## Conclusion

In this work, we evaluated the photocatalytic activity of two surface-modified dye-sensitized photocatalysts, **$H^+$-DSP** and **$Zr^{4+}$-DSP**, in the presence of $[SiV^{IV}W_{11}O_{40}]^{6-}$ or $[SiW_{11}O_{39}Mn^{II}(H_2O)]^{6-}$ (**$V^{IV}$-POM** or **$Mn^{II}$-POM**, respectively) as the RRED to find an effective interaction for one-way electron transfer from the electron mediator to the photocatalyst. **$H^+$-DSP**, comprising phosphonate groups on the photocatalyst surface, exhibited complete one-electron oxidation of **$V^{IV}$-POM** with 0.39% apparent quantum yield in the initial hour (*i*AQY) in both HCl and phosphate buffer aqueous solutions, even in the low concentration of 1 mM **$V^{IV}$-POM**. This *i*AQY value was comparable to that in higher concentrations of less charged RREDs (0.5 M $I^-$ and 16.4 mM $[Co(bpy)_3]^{2+}$), suggesting that stronger electrostatic interaction between the highly and negatively charged POM and photocatalyst surface can promote the forward electron transfer process. In contrast, the *i*AQY of **$Zr^{4+}$-DSP** in HCl aq was only 0.05%, owing to energy transfer deactivation by the surface-immobilized **$V^{IV}$-POM**, whereas almost the same activity (*i*AQY = 0.39%) was retained in the phosphate buffer solution. This deactivation process was further supported by the result that **$Zr^{4+}$-DSP** maintained almost the same activity in the HCl aq solution when **$V^{IV}$-POM** was replaced by the visible-light-transparent **$Mn^{II}$-POM**, which was also immobilized on the **$Zr^{4+}$-DSP** surface. These results suggest that to achieve efficient one-way electron transfer at the photocatalyst–mediator interface it is crucial to (1) ensure the driving force for the forward electron transfer and (2) eliminate non-favorable energy transfer quenching. Specifically, the accumulation of visible-light-transparent electron donors on the $H_2$ evolving photocatalyst surface should be a promising method for efficient one-directional electron transfer in the Z-scheme water splitting system.

## Experimental Section

### Essential materials and syntheses

Caution! *Although we did not come across any difficulties, most of the chemicals used in this study are potentially harmful and should be used in small quantities and handled with care in a fumehood.* All commercially available starting materials were used as received without further purification. $Pt/K_xH_{4-x}Nb_6O_{17}$, $K_6[SiV^{IV}W_{11}O_{40}]$ **($V^{IV}$-POM)**, $K_5[SiV^{V}W_{11}O_{40}]$ **($V^{V}$-POM)**, and $K_6[SiW_{11}O_{39}Mn^{II}(H_2O)] \cdot nH_2O$ (**$Mn^{II}$-POM**) were synthesized according to previously reported methods,[11,36] with some modifications. Ru(II) PSs (**RuCP**[6], and **RuP**[6])[44,45] and Ru(II)-dye-double-layered $Pt/K_xH_{4-x}Nb_6O_{17}$ nanoparticles (**$Zr^{4+}$-DSP** and **$H^+$-DSP**) were

prepared according to our previously reported method[35] (see the Supporting Information for details). The immobilized amounts of Ru(II) PSs were estimated by UV-vis absorption analysis of the supernatant solutions isolated after the immobilization reaction (Figure S2 and Table S1). Further characterization was conducted by powder X-ray diffraction (PXRD) measurement, suggesting that the layered structure of $K_xH_{4-x}Nb_6O_{17}$ was successfully retained after immobilization of Zr-**RuCP$^6$**-Zr-**RuP$^6$** layer (Figure S9).

**Measurements**

$^1$H-NMR spectra were recorded at 293 K on an JEOL ECZ-400S NMR spectrometer. UV−vis absorption spectra were recorded on a Shimadzu UV-2400PC spectrophotometer. Luminescence spectra were recorded on a JASCO FP-6600 or FP-8600 spectrofluorometer at 298 K. Each sample solution was deoxygenated by $N_2$ bubbling for 30 min at 298 K. Energy-dispersive XRF spectra were recorded using a Bruker S2 PUMA analyzer.

**Photocatalytic water reduction reaction**

For all experiments, 1 mM $K_6[SiV^{IV}W_{11}O_{40}]$ (**V$^{IV}$-POM**) or $K_6[SiW_{11}O_{39}Mn^{II}(H_2O)] \cdot nH_2O$ (**Mn$^{II}$-POM**), as the RRED, with HCl aqueous solution or 40 mM phosphonate buffer aqueous solution (pH = 3) was used to ensure the stable redox behavior of the POM species during photocatalytic reaction (Figure S10).[36] Under dark conditions, the POM solution containing **Zr$^{4+}$-DSP** or **H$^+$-DSP** nanoparticles (100 μM Ru(II) dye) was placed into an in-house made Schlenk flask-equipped quartz cell (volume: 265 mL) with a small magnetic stirring bar. Each sample flask was doubly sealed with rubber septa. This mixed solution was deoxygenated by Ar bubbling for 1 h. The flask was then irradiated from the bottom with a blue LED lamp (λ = 460 ± 15 nm; 70 mW; Opto Device Lab. Ltd., OP6-4710HP2). The temperature was controlled at 293 K using a homemade aluminum water-cooling jacket with a water circulating temperature controller (EYELA CCA-1111). The gas samples (0.6 mL) for each analysis were collected from the headspace using a gastight syringe (1 mL, Valco Instruments Co. Inc.). The amount of evolved $H_2$ was determined using a gas chromatograph (Agilent 490 Micro Gas Chromatograph). The turnover number and frequency per one PS (PS TON and PS TOF, respectively) were estimated from the amount of evolved $H_2$, which requires two photoredox cycles of Ru(II) PS to reduce one water molecule. Each photocatalytic $H_2$ evolution reaction was conducted thrice under the same conditions and the average value with standard deviation is reported. The detection limit of this gas chromatography analysis for $H_2$ gas was 0.005 μmol. The apparent quantum yield (AQY) was calculated using the following equation:

$$AQY = N_e/Np = 2N_{H2}/ N_p,$$

where $N_e$ represents the number of reacted electrons, $N_{H2}$ is the number of evolved $H_2$ molecules, and $N_p$ is the number of incident photons.

## Acknowledgements

This study was supported by the ENEOS Hydrogen Trust Fund, Casio Science Promotion Foundation, Iwatani Naoji Foundation, JSPS KAKENHI (grant numbers JP20H05082, 22K19039), and Hokkaido University DX Doctoral Fellowship (grant number JPMJSP2119).

**Keywords:** Water splitting • Photocatalysis • Dye sensitization • Surface modification • Polyoxometalate

[1] S. Acharya, D.K. Padhi, K. M. Parida, *Catal. Today* **2020**, *353*, 220-231.

[2] M. Graetzel, *Acc. Chem. Res*. **1981**, *14*, 376-384.

[3] Y. Ma, X. Wang, Y. Jia, X. Chen, H. Han, C. Li, *Chem. Rev*. **2014**, *114*, 9987-10043.

[4] A. Kudo, Y. Miseki, *Chem. Soc. Rev*. **2009**, *38*, 253-278.

[5] X. Fang, S. Kalathil, E. Reisner, *Chem. Soc. Rev*. **2020**, *49*, 4926-4952.

[6] A. Nakada, S. Nishioka, J. J. Vequizo, K. Muraoka, T. Kanazawa, A. Yamakata, S. Nozawa, H. Kumagai, S. Adachi, O. Ishitani, K. Maeda, *J. Mater. Chem. A* **2017**, *5*, 11710-11719.

[7] M. J. Fang, C. Tsao, Y. J. Hsu, *J. Phys. D: Appl. Phys.* **2020**, *53*, 143001-143033.

[8] H. Kumagai, R. Aoyagi, K. Kato, A. Yamakata, M. Kakihata, H. Kato, *ACS Appl. Energy Mater.* **2021**, 2056-2060.

[9] Q. Wang, T. Hisatomi, Q. X. Jia, H. Tokudome, M. Zhong, C. Z. Wang, Z. H. Pan, T. Takata, M. Nakabayashi, N. Shibata, Y. B. Li, I. D. Sharp, A. Kudo, T. Yamada, K. Domen, *Nat. Mater.* **2016**, *15,* 611-615.

[10] Y. Zhang, J. Qi, Y. Kong, Y. Zhao, S. Chen, D. Li, W. Liu, Y. Chen, T. Xie, J. Cui, K. Domen, F. Zhang, *Nat. Commun*. **2022**, *13*, 484.

[11] R. Abe, K. Shinmei, N. Koumura, K. Hara, B. Ohtani, *J. Am. Chem. Soc.* **2013**, *135*, 16872-16884.

[12] R. Abe, K. Shinmei, K. Hara, B. Ohtani, *Chem. Commun*. **2009**, *2009*, 3577-3579.

[13] R. Abe, K. Sayama, H. Arakawa, *J. Photochem. Photobiol., A* **2004**, *166*, 115-122.

[14] E. S. D. Silva, N. M. M. Moura, G. P. M. S. Neves, A. Coutinho, M. Prieto, C. G. Silva, J. Faria, *Appl. Catal., B* **2018**, *221*, 56-59.

[15] J. Warnan, J. Willkomm, J. N. Ng, R. Godin, S. Prantl, J. R. Durrant, E. Reisner, *Chem. Sci.* **2017**, *8*, 3070-3079.

[16] A. M. Deetz, G. J. Meyer *JACS Au* **2022**, *2*, 985–995.

[17] L. T. Gautier, M. D. Turlington, S. A. M. Wehlin, A. B. Maurer, M. D. Brady, W. B. Swords, G. J. Meyer, *Chem. Rev*. **2019**, *119*, 4628-4683.

[18] H. Kusama, T. Funaki, N. Koumura, K. Sayama, *Chem. Chem. Phys*. **2014**, *16*, 16166-16175.

[19] H. Kusama, *J. Photochem. Photobiol., A* **2018**, *365*, 110-118.

[20] A. Kobayashi, S. Takizawa, M. Hirahara, *Coord. Chem. Rev*. **2022**, *467*, 214624–22083.

[21] W. Wang, J. Chen, C. Li, W. Tian, *Nat. Commun.* **2014**, *5*, 4647-4654.

[22] J. Lee, D. Won, W. Jung, H. Son, C. Pac, S. O. Kang, *Angew. Chem., Int. Ed.* **2017**, *56*, 976-980.

[23] E. Aslan, M. K. Gonce, M. Z. Yigit, A. Sarilmaz, E. Stathatos, F. Ozel, M. Can, I. H. Patir, *Appl. Catal., B* **2017**, *220*, 320-327.

[24] A. Tiwari, N. V. Krishna, L. Giribabu, U. Pal, *J. Phys. Chem. C* **2018**, *122*, 495-502.

[25] F. Yu, S. Cui, X. Li, Y. Peng, Y. Yu, K. Yun, S. Zhang, J. Li, J. Liu, J. Hua, *Dyes Pigm.* **2017**, *139*, 7-18.

[26] Y. Sun, Y. Sun, C. Dall'Agnese, X. Wang, G. Chen, O. Kitao, H. Tamiaki, K. Sakai, T. Ikeuchi, S. Sasaki, *ACS Appl. Energy Mater.* **2018**, *1*, 2813-2820.

[27] T. Oshima, S. Nishioka, Y. Kikuchi, S. Hirai, K. Yanagisawa, M. Eguchi, Y. Miseki, T. Yokoi, T. Yui, K. Kimoto, K. Sayama, O. Ishitani, T. E. Mallouk, K. Maeda, *J. Am. Chem. Soc.* **2020**, *142*, 8412-8420.

[28] A. Nakada, T. Uchiyama, N. Kawakami, S. Nishioka, R. Kamata, H. Kumagai, O. Ishitani, Y. Uchimoto, K. Maeda, *ChemPhotoChem* **2019**, *3*, 37-45.

[29] M. V. Sheridan, Y. Wang, D. Wang, L. T. Gautier, C. J. Dares, B. D. Sherman, T. J. Meyer, *Angew. Chem. Int. Ed.* **2018**, *57*, 3449-3453.

[30] N. Yoshimura, A. Kobayashi, M. Yoshida, M. Kato, *Bull. Chem. Soc. Jpn*. **2019**, *92*, 1793-1800.

[31] N. Yoshimura, A. Kobayashi, W. Genno, T. Okubo, M. Yoshida, M. Kato, *Sustainable Energy Fuels* **2020**, *4*, 3450-3457.

[32] N. Yoshimura, A. Kobayashi, M. Yoshida, M. Kato, *Chem. Eur. J*. **2020**, *26*, 16939-16946.

[33] N. Yoshimura, M. Yoshida, M. Kato, A. Kobayashi, *Inorg. Chem.* **2022**, *61*, 11095-11102.

[34] S. Nishioka, K. Hojo, L. Xiao, T. Gao, Y. Miseki, S. Yasuda, T. Yokoi, K. Sayama, T. E. Mallouk, K. Maeda, *Sci. Adv*. **2022**, *8*, 9115.

[35] N. Yoshimura, A. Kobayashi, T. Kondo, R. Abe, M. Yoshida, M. Kato, *ACS Appl. Energy Mater.* **2021**, *4*, 14352-14362.

[36] O. Tomita, H. Naito, A. Nakada, M. Higashi, R. Abe, *Sustainable Energy Fuels* **2022**, *6*, 664-673.

[37] Y. Iwase, O. Tomita, H. Naito, M. Higashi, R. Abe, *J. Photochem. Photobiol., A* **2018**, *356*, 347-354.

[38] K. Tsuji, O. Tomita, M. Higashi, R. Abe, *ChemSusChem* **2016**, *9*, 2201-2208.

[39] J. Lei, J. Yang, T. Liu, T.; R. Yuan, D. Deng, M. Zheng, J. Chen, L. Cronin, Q. Dong, *Chem. Eur. J.* **2019**, *25*, 11432-11436.

[40] Y. B. M'Barek, T. Rosser, J. Sum, S. Blanchard, F. Volatron, G. Izzet, R. Salles, J. Fize, M. Koepf, M. Chavarot-Kerlidou, V. Artero, A. Proust, *ACS Appl. Energy Mater.* **2020**, *3*, 163-169.

[41] H. E. Moll, F. A. Black, C. J. Wood, A. Al-Yasari, A. Marri, I. V. Sazanovich, E. A. Gibson, J. Fielden, *Phys. Chem. Chem. Phys.* **2017**, *19*, 18831-18835.

[42] H. Cruz, A. L. Pinto, J. C. Lima, L. C. Branco, S. Gago, *Mater. Lett.* **2020**, *6*, 100033-100038.

[43] Y. Zhang, J. Liu, S. Li, Z. Su, Y. Lan, *Energy Chem.* **2019**, *1*, 100021-100078.

[44] K. Hanson, M. K. Brennaman, A. Ito, H. Luo, W. Song, K. A. Parker, R. Ghosh, M. R. Norris, C. R. K. Glasson, J. J. Concepcion, R. Lopez, T. J. Meyer, *J. Phys. Chem. C* **2012**, *116*, 14837-14847.

[45] S. Furugori, A. Kobayashi, A. Watanabe, M. Yoshida, M. Kato, *ACS Omega* **2017**, *2*, 3901-3912.

## Entry for the Table of Contents

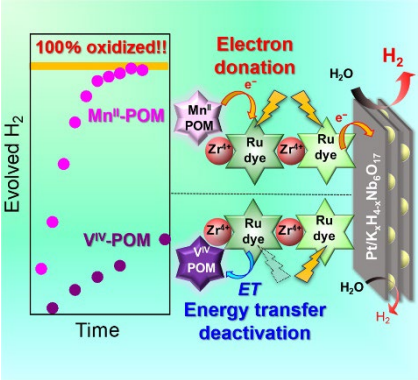


To accelerate electron transfer at photocatalyst-mediator interface, we developed the photocatalytic $H_2$ evolution system composed of $Zr^{4+}$-phosphonate-functionalized double-Ru-dye-layered $Pt/K_xH_{4-x}Nb_6O_{17}$ photocatalyst and highly charged polyoxometalate, M-POM (M = $V^{IV}$, $Mn^{II}$). Higher activity and complete oxidation of redox-reversible POM electron donor were achieved by using visible-light-transparent $Mn^{II}$-POM because of the negligible energy transfer deactivation from photoexcited Ru-dye to surface-immobilized POM.